Preparation of Alkanethiol Monolayers on Mild Steel Surfaces Studied with Sum Frequency Generation and Electrochemistry

Hongping Zhang, Casey Romero, and Steven Baldelli*

Department of Chemistry, University of Houston, Houston, Texas 77204

Received: May 27, 2005; In Final Form: June 25, 2005

An *n*-alkanethiol, octadecanethiol (ODT), monolayer was successfully prepared onto an oxide-free mild steel (MS) surface under cathodic polarization in a 0.1 M $LiCl/CH_3OH$ solution containing 1 mM ODT. Cyclic voltammetry (CV) and electrochemical impedance (EIS) and sum frequency generation (SFG) spectroscopy were applied to study and characterize the adsorption of ODT at a MS surface. In 0.1 M $LiCl/CH_3OH$ solution containing 1 mM ODT, CV of the MS electrode shows a dramatic decrease in charging current and a positive shift in oxidation potential when compared to a solution without ODT. The interfacial capacitance was obtained as 2.52 $\mu F/cm^2$ from the impedance data. An average chain tilt angle of 48° for the ODT molecules was deduced from the comparison of the interfacial capacitances of the ODT/MS and ODT/Au monolayers. X-ray photoelectron spectroscopy confirmed the formation of the ODT monolayer on mild steel. The ppp SFG spectrum of the ODT-modified MS features three strong methyl vibrational modes at 2877, 2943, and 2967 cm^{-1}, indicating the formation of the oriented and densely packed ODT monolayer. However, the appearance of the two weak CH_2 groups' vibrational modes at 2850 and 2914 cm^{-1} implies the presence of defects in the ODT monolayer. ODT/Au films were prepared to compare with the ODT/MS films. Orientation analysis of the air/solid interface suggests that the methyl group of ODT/Au films has a tilt angle of 30°, while the methyl group of ODT/MS films has a tilt angle of 23°. Water was found to have an impact on the shape of the SFG spectra of ODT/MS. This suggests that the solution penetrated through the defects to reach the MS surface.

Introduction

Self-assembled thiol monolayers (SAMs) have been extensively studied over the past two decades due to their tuning capability for the properties of metal surface and their numerous potential technological applications.[1−14] The substrates that have been used for depositing thiol SAMs mainly focus on noble or coinage metals such as gold,[1−6,8−12,14−17] silver,[1,15−19] platinum,[17,20−22] and copper.[1,7,15−17,23,24] Although engineering metals (iron, steel, etc.) have a wider utilization in modern industry, there are only a few reports concerning thiol SAMs on these metals.[25−29] A probable reason is that the surfaces of iron and steel are quite active and easily oxidized under ambient laboratory conditions. Volmer and co-workers reported cyclic voltammetry (CV) and X-ray photoelectron spectroscopy (XPS) studies of *n*-alkanethiol on an oxide-free iron surface under potential control.[25,26] They applied a negative potential to remove the native oxide layer of iron and then pulled the electrode through a liquid thiol phase that was above the aqueous electrolyte to form a monolayer on the iron surface. Recently, Ruan and co-workers deposited *n*-alkanethiol on stainless steel and characterized the monolayers by XPS and Fourier transform infrared spectroscopy (FTIR).[30]

Well-defined SAMs are densely packed and highly ordered. Usually, one can use grazing X-ray diffraction (XRD),[4] scanning tunneling microscopy (STM),[5,7] high-resolution electron energy-loss spectroscopy (HREELS),[31,32] and FTIR,[7,30,33−35] etc., to measure if the monolayer is ordered or not. Besides these, sum frequency generation (SFG) spectroscopy proves to be a direct and effective tool to deduce the orientated order of surface adsorbates.[36−54]

As a surface/interfacal sensitive molecular vibrational spectroscopic technique, SFG has been widely used to study molecular adsorption on metal surfaces such as Au, Ag, Pt, Cu, etc. However, few papers have concentrated on using SFG to study iron or steel surfaces.[43,55,56]

This work presents the results of SFG, XPS, electrochemical impedance spectroscopy (EIS), and cyclic voltammetry (CV) studies of the octadecanethiol (ODT) monolayer deposited on a mild steel surface under potential control in $LiCl/CH_3OH$ solution and compares them to Au/ODT surfaces. The SFG spectra of ODT monolayers formed at various potential control procedures were compared. These experiments suggest that the ODT molecules can self-assemble on the electrochemically reduced mild steel surface and form a well-defined monolayer.

Experimental Section

Materials. Octadecanethiol (ODT, $CH_3(CH_2)_{17}SH$, 98%) and methanol (99.9%, spectrophotometric grade) were purchased from Aldrich Chemical Corp. and used as received. Lithium chloride (LiCl, anhydrous, 99% min) was obtained from A Johnson Matthey Company. Mild steel (MS) rods (8 mm diameter, 10 mm length) were provided by Champion Technologies, Houston, TX.

Electrochemistry. The working electrode used was a MS rod which was mounted in a Teflon sheath exposing only the circular cross section (0.50 cm^2 surface area). After being polished by 1000 grit emery paper, the MS electrode was then sequentially polished with a 6, 3, and 1 μm diamond suspension.

* To whom correspondence should be addressed. E-mail: sbaldelli@uh.edu.

10.1021/jp052807p CCC: $30.25
Published on Web 07/23/2005

Then the electrode was rinsed, ultrasonicated with acetone for 5 min, and then rinsed with water from a Millipore A10 system (>18 MΩ·cm^2). Finally, the MS electrode was thoroughly rinsed with water and methanol before it was placed into the electrochemical cell. A platinum wire ring or mesh was used as the counter electrode. The reference electrode was a saturated calomel electrode (SCE). All electrochemical experiments were carried out in a three-electrode system glass cell. The cell was cleaned in a 1:1 mixture of nitric acid and sulfuric acid or baked in an oven at 570 °C over 1 h before each use.

All potential control for the ODT monolayer deposition was performed using an EG&G PAR M263A potentiostat/galvanostat. CV experiments were performed using the M263A potentiostat that was controlled by PowerCV software. EIS measurements were performed using the M263A potentiostat in combination with a PAR M5210 lock-in amplifier controlled by PowerSINE software. The frequency range used was from 10 kHz to 30 or 10 Hz at open circuit potential (OCP). The amplitude of the applied sinusoidal signal was 5 mV.

All solutions were purged with pure N_2 gas flow for approximately 15 min and kept bubbling during ODT deposition and EIS measurement before introducing working electrodes. Each EIS experiment was performed three times, and the results were averaged. The impedance data was fit to an equivalent circuit by ZSimpWin software.

ODT/MS Electrode Preparation Procedure. After pretreatment, the smooth and clean MS electrode was placed immediately into 30 mL of 0.1 M LiCl/CH_3OH solution in the electrochemical cell, and a negative potential (−1.2 V) was applied for 20 min to remove the oxide layer on the surface. Then, 20 mL of 0.1 M LiCl/CH_3OH solution containing 14.3 mg of ODT was injected into the cell under potential control. The final concentration of ODT was 1 mM. The potential was kept between −1.2 and −1.1 V for 1−2 h. We note that a longer assembly time does not obviously improve the quality of the film based on SFG results. The SFG spectra of a sample prepared in 2 h is similar to that of a sample prepared in 7 h for our experiments. The electrode was taken out from solution immediately after switching off the potential, thoroughly rinsed with methanol, ultrasonicated in methanol for 5 min in order to remove physically adsorbed ODT molecules, rinsed with methanol again, and dried in a pure N_2 gas stream. SFG data was collected in air or water within 10 min of preparation. All experiments were carried out at room temperature.

ODT/Au Modified Electrodes Preparation. For comparison and reference, ODT monolayers on a Au surface were routinely prepared, and the ODT/Au electrodes were studied using EIS and SFG.

Finely polished (with 0.05 μm alumina paste) gold disk electrodes with 8 mm diameter were ultrasonicated in acetone, rinsed with water, followed by cleaning in fresh Piranha solution (1:3 v/v H_2O_2/H_2SO_4), rinsed with Millipore water and methanol, and dried with a stream of pure N_2 gas. Then they were immediately placed into a 0.1 M LiCl/CH_3OH solution containing 1 mM ODT for several hours. The ODT-modified Au electrode was rinsed with methanol, ultrasonicated in methanol, and dried with N_2 gas before the experiment.

XPS Instrument. XPS spectra were recorded on a PHI (Physical Electronics Inc., USA) 5750 X-ray photoelectron spectrometer using a mono Al X-ray source operated at 350 W. The pass energy for the multiplex scan was 23.5 eV. The sample was tilted 45° relative to the detector. All binding energies were referenced to the C_{1s} peak at 285 eV.

SFG Instrument. The SFG spectrometer used is homemade; details of the setup have been described elsewhere.[52] An EKSPLA (Lithuania) Nd:YAG laser at 1064 nm with a 25 ps long pulse and a 20 Hz repetition rate was used as the pump source for an optical parametric generation/optical parametric amplification (OPG/OPA) (LaserVision) system. The OPG/OPA produced a tunable IR beam which can be scanned from 2.5 to 5 μm (4000−2000 cm^{-1}) using nonlinear crystals $KTiOPO_4$ (KTP) and $KTiOAsO_4$ (KTA). The visible beam was produced via the 1064 nm beam being frequency doubled to 532 nm in a KTP crystal. The optical geometry adopted a copropagating configuration in which incidence angles of the visible and IR beams are 45° and 60°, respectively. The visible and IR beams were overlapped both spatially and temporally at the metal surface. The SFG signal reflected from the metal surface was filtered from a 532 nm input beam using an interference filter and monochromator and collected with a photomultiplier tube (PMT). A reference IR signal reflected from metal surface was collected simultaneously for normalizing the SFG signal intensity. The change of polarization of the incident laser beams was accomplished with the use of $\lambda/2$ waveplates, and Glan-Laser polarizers were used to ensure the polarization combinations were correct for input and emitted beams. Two polarization combinations, ssp (s-polarized SFG, s-polarized visible, and p-polarized IR) and ppp, were acquired in the C−H stretching region from 2800 to 3100 cm^{-1} for each sample. The scan rate was 1 cm^{-1}/s with an average of 20 laser shots per data point. Each spectrum is an average of 5 or 10 scans. Each SFG spectrum was fitted in Origin 6.0 using a nonlinear curve fitting function with instrumental weighing for the error bars which represents the standard deviation of the fit. The following function was used to fit the SFG spectra

$$I_{\mathrm{SFG}} \propto |\chi^{(2)}_{\mathrm{NR}} + \chi^{(2)}_{\mathrm{R}}|^2 = |\chi^{(2)}_{\mathrm{NR}} + \sum_q \frac{A_q}{\omega_{\mathrm{IR}} - \omega_q + i\Gamma_q}|^2 \quad (1)$$

where $\chi^{(2)}_{\mathrm{NR}}$ and $\chi^{(2)}_{\mathrm{R}}$ are the nonresonant susceptibility attributed to the metal substrate and the resonant susceptibility attributed to adsorbed molecules, respectively. q is the qth resonant vibrational mode of the adsorbates. A_q, ω_{IR}, ω_q, and Γ_q are the amplitude, scanning IR frequency, the qth resonant vibrational frequency of the adsorbates, and line width, respectively.

SFG Orientation Calculation. The intensity of the sum frequency beam depends on the intensities of the incident beams, E_{vis} and E_{IR}, and the second-order nonlinear susceptibility, $\chi^{(2)}$.

$$I_{\mathrm{SFG}} \approx |K_{\mathrm{SFG}}\chi^{(2)}K_{\mathrm{vis}}E_{\mathrm{vis}}K_{\mathrm{IR}}E_{\mathrm{IR}}|^2 \quad (2)$$

To relate experimental SFG intensity to $\chi^{(2)}$ accurately, the macroscopic local-field corrections, also known as Fresnel coefficients, for the incident fields and for the sum frequency field created at the interface must be known. The local-field factors take into account the reflection, refraction, and enhancement of the fields due to the presence of the interface. The local field factors, K_{xx}, K_{yy}, and K_{zz}, relating to the input visible and IR electric fields and output sum frequency field are as follows[57]

$$K_{xx} = \frac{E_{\mathrm{surface}}}{E_{\mathrm{laser}}}|_x = \frac{2n_1(\omega)\cos\theta_2}{n_2(\omega)\cos\theta_1 + n_1(\omega)\cos\theta_2}\cos\theta_1 \quad (3)$$

$$K_{yy} = \frac{E_{\mathrm{surface}}}{E_{\mathrm{laser}}}|_y = \frac{2n_1(\omega)\cos\theta_1}{n_1(\omega)\cos\theta_1 + n_2(\omega)\cos\theta_2} \quad (4)$$

$$K_{zz} = \frac{E_{\text{surface}}}{E_{\text{laser}}}|_z = \frac{2n_2(\omega)\cos\theta_1}{[n_2(\omega)\cos\theta_1 + n_1(\omega)\cos\theta_2]}\frac{{n_1}^2(\omega)}{{n_m}^2(\omega)}\sin\theta_1 \quad (5)$$

where θ_1 is the incident angle and θ_2 is the transmitted angle through the media. n_1, n_2, and n_m are the refractive indices of media 1 and 2 and the monolayer, respectively (see Figure 8). The refractive indices are wavelength dependent and must be determined for both input and output beams. p-Polarized light has contributions in two directions, *x* and *z*. K_{xx} and K_{zz} are the two components of p-polarized light once they have been separated. ${n_1}^2/{n_m}^2$ has been added to K_{zz} to make corrections due to the polarization sheet of the interface.[58] The refractive index of a material is a macroscopic property, which has led to much debate about how to calculate the refractive index of the monolayer, n_m.[42,59]

For metal surfaces it is more straightforward to deal with the Fresnel equations only in terms of the incident angle. Most metals have a large imaginary component of their refractive index at frequencies below the plasma frequency. This causes the calculation of the transmitted angle to be ambiguous. Since the Fresnel equations can be represented as a function of the amplitude reflection coefficients

$$K_{zz} = E_p^i(1 + r_p)\sin\theta_1\frac{{n_1}^2}{{n_m}^2} \quad (6)$$

$$K_{xx} = E_p^i(1 - r_p)\cos\theta_1 \quad (7)$$

$$K_{yy} = E_s^i(1 + r_s) \quad (8)$$

where

$$r_s = \frac{n_1\cos\theta_1 - n_2\cos\theta_2}{n_1\cos\theta_1 + n_2\cos\theta_2} \quad (9)$$

$$r_p = \frac{n_2\cos\theta_1 - n_1\cos\theta_2}{n_1\cos\theta_2 + n_2\cos\theta_1} \quad (10)$$

Snell's law

$$n_1\sin\theta_1 = n_2\sin\theta_2 \quad (11)$$

can then be used to represent the amplitude reflection coefficients in terms of incident angle only.

$$r_s = \frac{E_\perp^r}{E_\perp^i} = \frac{n_1\cos\theta_1 - ({n_2}^2 - {n_1}^2\sin^2\theta_1)^{1/2}}{n_1\cos\theta_1 + ({n_2}^2 - {n_1}^2\sin^2\theta_1)^{1/2}} \quad (12)$$

$$r_p = \frac{E_{ll}^r}{E_{ll}^i} = \frac{{n_2}^2\cos\theta_1 - n_1({n_2}^2 - {n_1}^2\sin^2\theta_1)^{1/2}}{{n_2}^2\cos\theta_1 + n_1({n_2}^2 - {n_1}^2\sin^2\theta_1)^{1/2}} \quad (13)$$

The Fresnel equations shown above all take into account the polarization sheet's influence on both the incident and output electric fields strength at the surface. There is some ambiguity in the literature for the influence the polarization sheet has on both the input and output electric fields.[42,57,60−62] Because each system studied is different, the best way to take into account the significance of the monolayer is yet to be determined.

The sign of the Fresnel coefficients is determined by the coordinate system. The coordinate system used in this study was the same used for Shen et al.[57] In Figure 8, the *z*-coordinate is pointing down into the interface. Therefore, all the *z*-components of the electric fields of the Fresnel coefficients must be negative. For the *x*-components, the input fields are negative and the output field is positive. The sign of the Fresnel coefficients is important for calculating the relative sign of each susceptibility tensor in the ppp polarization combination contribution and will be explained below.

Monolayers that are isotropic in the plane of the surface only have four independent components of $\chi_{ijk}^{(2)}$: $\chi_{zxx}^{(2)} = \chi_{zyy}^{(2)}$, $\chi_{xzx}^{(2)} = \chi_{yzy}^{(2)}$, $\chi_{xxz}^{(2)} = \chi_{yyz}^{(2)}$, and $\chi_{zzz}^{(2)}$. Only four combinations of polarization allow sum frequency emission: ssp, ppp, sps, and pss. Each of these polarization combinations probes a different tensor element of $\chi_{ijk}^{(2)}$, except for the ppp combination which probes a combination of the tensor elements. For the ppp polarization combination, the sign of the Fresnel coeffients causes the interference terms arriving from the addition of four susceptibilities to interfere either constructively or destructively depending on the sign.

$$I_{ssp} \approx |\chi_{yyz}^{(2)}E_{vis}E_{IR}|^2 \quad (14)$$

$$I_{sps} \approx |\chi_{yzy}^{(2)}E_{vis}E_{IR}|^2 \quad (15)$$

$$I_{pss} \approx |\chi_{zyy}^{(2)}E_{vis}E_{IR}|^2 \quad (16)$$

$$I_{ppp} \approx |\chi_{zzz}^{(2)}E_{vis}E_{IR} + \chi_{zxx}^{(2)}E_{vis}E_{IR} + \chi_{xzx}^{(2)}E_{vis}E_{IR} + \chi_{xxz}^{(2)}E_{vis}E_{IR}|^2 \quad (17)$$

When metal surfaces are probed, the Fresnel coefficients cause the *x*- and *y*-components of the IR electric field at the surface to be much smaller than the *z*-component; therefore there are only two independent components of $\chi_{ijk}^{(2)}$: $\chi_{zzz}^{(2)}$, $\chi_{xxz}^{(2)} = \chi_{yyz}^{(2)}$. Sum frequency emission only occurs using polarization combinations with a *z*-component of the IR electric field, ssp and ppp.

$$I_{ssp} \approx |\chi_{yyz}^{(2)}E_{vis}E_{IR}|^2 \quad (18)$$

$$I_{ppp} \approx |\chi_{zzz}^{(2)}E_{vis}E_{IR} + \chi_{xxz}^{(2)}E_{vis}E_{IR}|^2 \quad (19)$$

$\chi^{(2)}$ is a macroscopic term which can be expressed in terms of the ensemble average of the microscopic hyperpolarizabilty tensor $\langle\beta\rangle$ by

$$\chi_R^{(2)} = N\langle\beta\rangle \quad (20)$$

where *N* is the total number of modes which contribute to the SFG signal. The hyperpolarizability is a product of the Raman

$$\beta_{abc} = \langle g|\alpha_{ab}|v\rangle\langle v|\mu_c|g\rangle \quad (21)$$

polarizability, α_{ab}, and the IR transition dipole moment of the molecule, μ_c. The hyperpolarizability tensors were calculated using the bond additivity model outlined by Hirose.[36] The microscopic quantities of the hyperpolarizability tensor are described in the molecule-fixed (*xyz*) axis system. To relate the β value with $\chi^{(2)}$, a coordinate transformation must be performed using the Euler matrix

$$\chi_{XYZ} = \sum_{xyz} U_{XYZ:xyz}\chi_{xyz} \quad (22)$$

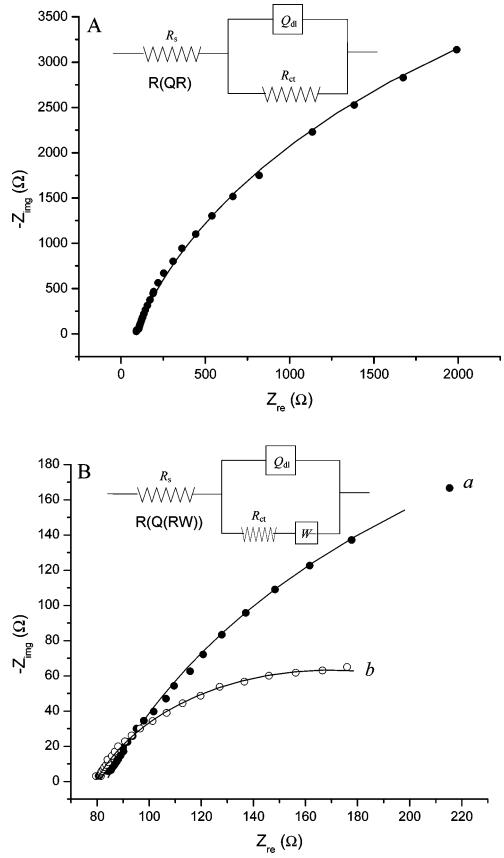

Figure 1. Nyquist impedance plots at open circuit potential and the fitted line: (A) gold in 0.1 M LiCl/CH_3OH solution containing 1 mM ODT from 10 kHz to 10 Hz; (B, part a) oxide-free mild steel in 0.1 M LiCl/CH_3OH solution from 10 kHz to 30 Hz, (B, part b) oxide-free mild steel in 0.1 M LiCl/CH_3OH solution containing 1 mM ODT from 10 kHz to 30 Hz.

The components of the transformation matrix depend on the Euler angles (θ, ϕ, χ) which relate the molecular and laboratory-fixed coordinate systems. This paper will be concerned with the stretching modes of the methyl group of the ODT monolayer. The methyl group is assumed to have C_{3v} symmetry, and the methyl group has free rotation along the molecular axis. For molecules with C_{3v} symmetry, only the components of the hyperpolarizability tensor β_{aac},β_{bbc},β_{ccc} have contributions from symmetric vibrations. Asymmetric vibrations contain contributions from the following hyperpolarizabiltiy tensor elements, β_{aca},β_{bcb},β_{caa},β_{cbb}. The other tensor elements ascribed to the asymmetric vibrations integrate to zero when free rotation of the methyl group is assumed. This allows the components of the transformation matrix to be averaged over ϕ and χ which leads to an equation which is only a function of the tilt angle θ. These curves are then compared with the intensities of the vibrations measured by curve fitting the spectra to give an estimated orientation.

3. Results and Discussion

3.1. ODT/Au Reference Data. Figure 1A shows one of the Nyquist plots of an ODT/Au electrode in ODT-containing 0.1 M LiCl/CH_3OH solution at OCP. The EIS spectrum appears as a compressed semicircle rather than a straight line. Equivalent circuits such as RC and R(QR) are usually used to fit impedance data of thiolate on a gold surface,[63−66] where R, C, and Q are the resistor, capacitor, and constant phase element, respectively. Parentheses denote the two elements that are in parallel. In this case, it was found that R(QR) was the best choice to fit the impedance data of the ODT/Au system. Here, a constant phase element (CPE,Q) was used instead of a double layer capacitor to get more precise fit results. For a solid electrode in a solution absent of a suitable redox couple, the CPE phenomenon has been often observed due to the "dispersing effect" which may arise from microscopic roughness.[64] The fitting results in Figure 1A are 5.12 $\mu\Omega^{-1}\cdot cm^{-2}\cdot s^n$, 0.87, 22.0 $k\Omega\cdot cm^{-2}$ for Q, n, and R_{ct}, respectively. On the other hand, it is capacitance, C, rather than (CPE,Q), which correlates with the thickness of thin films adsorbed on electrode surfaces[65−67]

$$C = \frac{\epsilon\epsilon_0}{d} \propto \frac{1}{d} \tag{23}$$

where ϵ, ϵ_0, and d are the dielectric constant of the thiol molecule, the permittivity of free space, and the thickness of the film, respectively. Because both ϵ and ϵ_0 are constant for a certain species, so C is inversely proportional to d. Recently, Hsu and Mansfeld reported an approach from CPE to C for a (QR) loop in which a CPE is parallel to a resistance[68]

$$C = Q_0(2\pi f_{max})^{n-1} \tag{24}$$

Here f_{max} is the frequency at which the imaginary part of the impedance has a maximum. Although there is no measured f_{max} value in plot a of Figure 1, we applied the fit parameters of plot a to the equivalent circuit, R(QR), and obtained a simulated f_{max} of 259.6 Hz. Substituting this simulated f_{max} value and fit parameters Q_0 and n into eq 24, a capacitance value of C = 1.96 $\mu F/cm^2$ was obtained. Note the use of the geometric area (0.5 cm^2) of the Au disk as the electrode surface area.

SFG spectra of the ODT monolayer on the Au surface are consistent with the spectral data available in the literature. In our case, the resonances appear as dips rather than peaks. In the reports of Hines,[40] Tanaka,[44] and Himmelhaus,[47] the resonances of the ODT monolayers on gold are dips, while Bain[37,39] reported peaks. In fact, for the adsorbates on metal substrates, the line shape of the resonant SFG signal, peak, or dip, depends on the phase difference of the nonresonance and resonance susceptibilities.

$$\begin{aligned} I_{SF} \propto |P^{(2)}| \propto |\chi^{(2)}_{NR} + \chi^{(2)}_{R,q}|^2 \\ = ||\chi^{(2)}_{NR}|(\cos\varphi + i\sin\varphi) + |\chi^{(2)}_{R,q}|[\cos\delta_q(\omega) + \\ i\sin\delta_q(\omega)]|^2 \\ = |\chi^{(2)}_{NR}|^2 + |\chi^{(2)}_{R,q}|^2 + 2|\chi^{(2)}_{NR}|\cdot|\chi^{(2)}_{R,q}| \\ \cos[\varphi - \delta_q(\omega)] \end{aligned} \tag{25}$$

Here, j is the phase of $\chi^{(2)}_{NR}$ and $d_q(\omega)$ is the phase of the qth $\chi^{(2)}_{R,q}$. For some metals such as gold, copper, and mild steel, etc., $\chi^{(2)}_{NR}$ is generally greater than $\chi^{(2)}_{R,q}$, and the line shape is therefore determined by the interference item (the third term in eq 25).[55,69] The sign of $\cos[\varphi - \delta_q(\omega)]$ therefore determines the resonance SFG signal appearing as a peak or dip. On the basis of eq 1, one can deduce that, at vibrational resonance ($\omega_{IR} = \omega_q$), $\chi^{(2)}_{R,q}$ is purely an imaginary number, meaning its phase must be $+\pi/2$ or $-\pi/2$. Consequently, $\cos[\varphi - {}_q(\omega_q)]$ may be equal to $\sin\varphi$ or $-\sin\varphi$. Hence, the value of the nonresonant phase and the sign of the $\sin\varphi$ function provide us a simple and clear way to understand the various line shapes of SFG spectra on metal substrates. Miranda,[58] Chou,[51] and Bain[70] and co-workers have presented simulation for the effect of the phase of nonresonance on the SFG line shape.

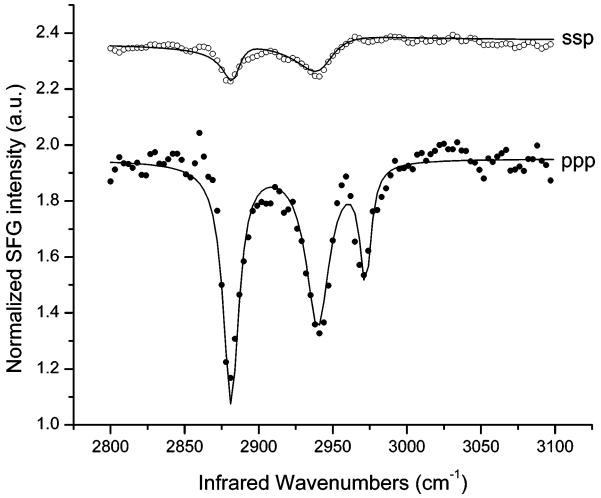

Figure 2. Typical SFG spectra of an ODT monolayer modified gold surface. The solid line is the curve of fit on eq 1. The ssp spectrum has been offset vertically +1.1 for clarity.

The phase of the nonresonance depends not only on the material of the substrate but also on the laser geometric configuration and the polarization combination. Since the local IR field sensed by the adsorbed molecules is essentially along the *z* axis (surface normal) due to the large imaginary dielectric constant of the metal, while the IR field in the metal is mostly along the *x* axis (*xz* and *xy* planes are the incident plane and surface, resepectively).[40,71] Consequently, for a ppp SFG spectrum, the resonant signal of adsorbed molecules is dominated by $\chi^{(2)}_{zzz}$ and $\chi^{(2)}_{xxz}$ which have the same sign in both of the copropagating and the counterpropagating configurations. However, $\chi^{(2)}_{zxx}$ and $\chi^{(2)}_{xzx}$ dominate the nonresonant signal of the substrates. They have a reversed sign in the two different laser geometries.[40,44] This means that the phase of the nonresonant is changed by π with the changing of the laser configuration. The case is different for the ssp SFG spectrum, because only the $\chi^{(2)}_{yyz}$ component, which has same sign in both laser geometries, contributes to the ssp signal. So ssp SFG spectra should have the same features in both of the configurations.

In a word, the resonant line shape depends on the phase difference of the nonresonance and resonance susceptibilities. Polarization combination and geometry can change the resonant line shape through changing the phase of the nonresonance, while the dipole direction of the adsorbates only changes the phase of the resonance by π. This is verified by previous reports and our fitting results of SFG spectra of the ODT monolayer at the Au and MS surface.

Figure 2 shows the typical SFG spectra of an ODT monolayer modified Au surface. The ppp spectrum has three main resonances, and the ssp spectrum has two main resonances. Note, in the ssp spectrum of ODT/Au, resonances appear as dips as they do in countergeometry. All of these dips are attributed to the terminal methyl group of the ODT molecules. On the basis of the literature,[40−45,47,48,50,52] the peaks at 2879, 2938, and 2967 cm^{-1} are assigned to the symmetric, Fermi resonance, and antisymmetric CH-stretching vibrational modes of the terminal CH_3 group, respectively. The absence of the contribution from methylene modes in the SFG spectra indicates the ODT monolayer was densely packed and highly ordered at the Au surface. The fitting result reveals that the phase of the nonresonance for the Au substrate are $\varphi_{Au,ppp} = 88°$ (≈90°) and $\varphi_{Au,ssp} = 61°$ (≈60°) for ppp and ssp SFG spectra, respectively. These values are consistent with the report of Bain et al.[38,41] The only difference is the sign of the phase angles that can be easily explained by the difference of the laser configuration and the opposite assignment to the sign of the $\chi^{(2)}_{R,q}$ at resonance.

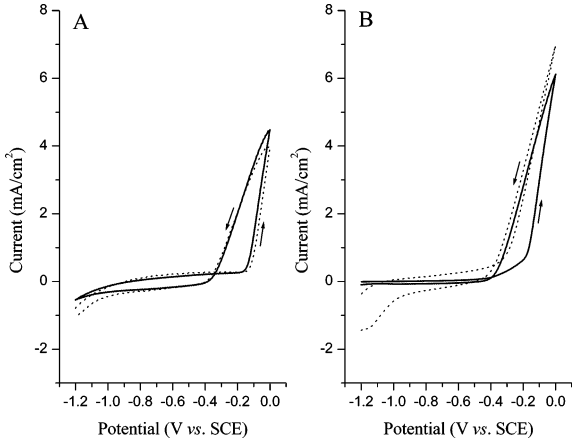

Figure 3. Cyclic voltammograms of a nonreduced (A) and a reduced (B) mild steel electrode in 0.1 M LiCl/CH_3OH solution with (solid line) and without (dotted line) 1 mM ODT, scan rate 50 mV/s.

3.2. CV of Mild Steel. It is well-known that a thiol monolayer can be easily formed at a noble metal surface by cleaving the S−H bond and the formation M(I)−S bond.[13,72] Therefore, a nonnoble metal is generally not a good substrate for thiol molecules to adsorb unless the oxide layer is removed. CV is a quite simple and fast method to evaluate the adsorption behavior of thiols at an electrode surface. When a long chain alkane thiol monolayer is deposited on an electrode, the charging current in the CV decreases dramatically and hardly changes with the potential in the region of the non-Faradic current. As shown in Figure 3A, the presence of the ODT almost has no influence on the charging current and onset oxidized potential of a nonreduced MS electrode in 0.1 M LiCl/CH_3OH solution. It implies that the adsorption of ODT at a nonreduced MS surface is very weak. However, the presence of the ODT significantly changed the CV behavior of the oxide-free MS electrode as shown in Figure 3B. The electric double layer charging current reduced sharply due to the formation of the ODT monolayer at the MS surface. Moreover, the onset oxidized potential of the MS positively shifts by about +150 mV showing a block effect on the oxidation process of MS. Feng[73] and Ma[74] have reported similar CV behaviors of the thiol-modified copper electrodes.

3.3. EIS of Mild Steel. In Figure 1B, plot a and plot b are the typical at−OCP Nyquist plots of the oxide-free MS electrodes after cathodic polarization at −1.2 V for 0.5 h in 0.1 M LiCl/CH_3OH solution without and with 1 mM ODT added, respectively. The equivalent circuits, R(QR) and R(Q(RW)) were used to fit plot a and plot b, respectively, where *W* is the Warburg impedance. In the case of MS in a solution containing ODT (represented by plot b), the average capacitance value for the ODT film was deduced as $C = 2.52\ \mu F/cm^2$ using eq 24. This value is very close to that of ODT/Au in our experiment ($1.96\ \mu F/cm^2$). It confirmed the formation of the ODT monolayer at the MS electrode surface under electrochemical reduction. We presumed that the increase of *C* for ODT/MS resulted from a slightly greater tilt angle of the ODT molecules at the MS surface, which may imply a slightly lower packing density and the presence of defects. On the basis of this presumption, a simple geometric model, shown in Figure 4, was used to evaluate the average tilt angle of the ODT molecules at the MS surface. In this model, *l*, *d*, and α are the chain length of ODT molecules with an all-trans configuration, monolayer thickness, and the molecular chain tilt angle from the surface normal,

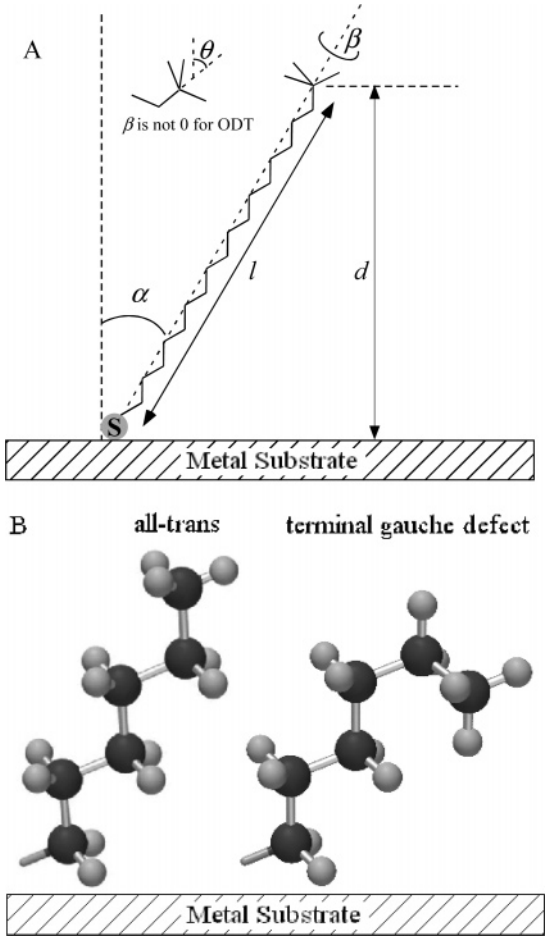

Figure 4. Schematic model for calculating the tilt angle of the ODT molecules adsorbed at oxide-free mild steel surface (A) and the all-trans and the simplest gauche model, terminal gauche conformations of a hydrocarbon chain (B).

respectively. Assuming l is independent of the orientation of the ODT molecules in a perfect monolayer, then we have

$$d = l \cos \alpha \propto \cos \alpha \tag{26}$$

Combining eq 23 and 26, we get

$$\cos \alpha \propto \frac{1}{C} \tag{27}$$

For a well defined thiol monolayer on a Au substrate, it is generally accepted that the chain tilt angle of the thiol molecules is about 30°.[1,75,76]

Hence, the average tilt angle of the ODT molecules at the MS surface can be deduced as

$$\cos \alpha_{ODT/MS} = \frac{C_{meas,ODT/Au}/A_{Au}}{C_{meas,ODT/MS}/A_{MS}} \cos \alpha_{ODT/Au} \tag{28}$$

Here, C_{meas} is the capacitance value measured from the EIS experiment. A_{Au} and A_{MS} are the surface area of the Au and MS electrodes, respectively. In our calculation, they are regarded as the same value due to the same geometric diameters. It gives $\alpha \approx 48°$ for ODT/MS. This result will be compared with the SFG calculation, and the detailed discussion will be presented later.

3.4. XPS of Mild Steel. To further verify the formation of the ODT monolayer at a MS surface, the MS electrodes with and without ODT modification were analyzed by XPS. Figure 5 shows the high-resolution spectra in the range of S_{2p}. For an unmodified MS electrode, there is no comparable binding energy peak assignable to sulfur in this range (Figure 5A). However, the XPS spectrum of the ODT-modified MS (Figure 5B) shows an obvious binding energy peak at 162.1 eV which is assigned to S_{2p} of the thiolates. Moreover, ODT deposition led to a more intense C_{1s} binding energy peak and a weaker Fe_{2p} peak in XPS spectra (not shown) compared to the bare MS. All of these results support the formation of an ODT monolayer at MS. These results agree well with Ruan's report.[30] There is no binding energy peak belonging to sulfate or sulfite between 165 and 171 eV meaning that the ODT monolayer on MS is stable in air.

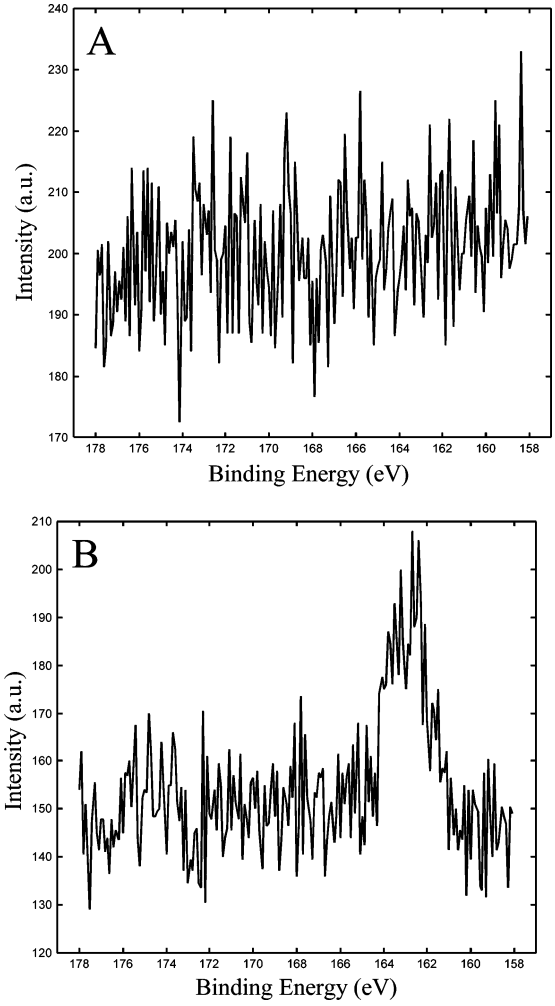

Figure 5. S_{2p} XPS spectra of bare mild steel (A) and ODT modified mild steel (B).

3.5. SFG of ODT Modified Mild Steel Surfaces. Figure 6 shows the SFG spectra of the MS electrodes that have undergone various treatments in 0.1 M LiCl/CH_3OH solution. Figure 6A is the SFG spectra of an oxide-covered MS electrode after being immersed in 0.1 M LiCl/CH_3OH solution containing 1 mM ODT for 2 h. There is no significant resonance feature due to a low surface density or random orientation of the ODT molecules at an oxidized MS electrode. The CV results (see Figure 3A) support the former, indicating a weak adsorption of ODT molecules at an oxide-covered MS surface.

SFG spectra (shown in Figure 6B) of a MS electrode, which was immersed in 0.1 M LiCl/CH_3OH solution at −1.2 V for 2 h, show only a very small resonant feature at 2940 cm^{-1}, demonstrating that the solvent, CH_3OH, does not contribute significantly to the SFG spectra of the ODT monolayer under

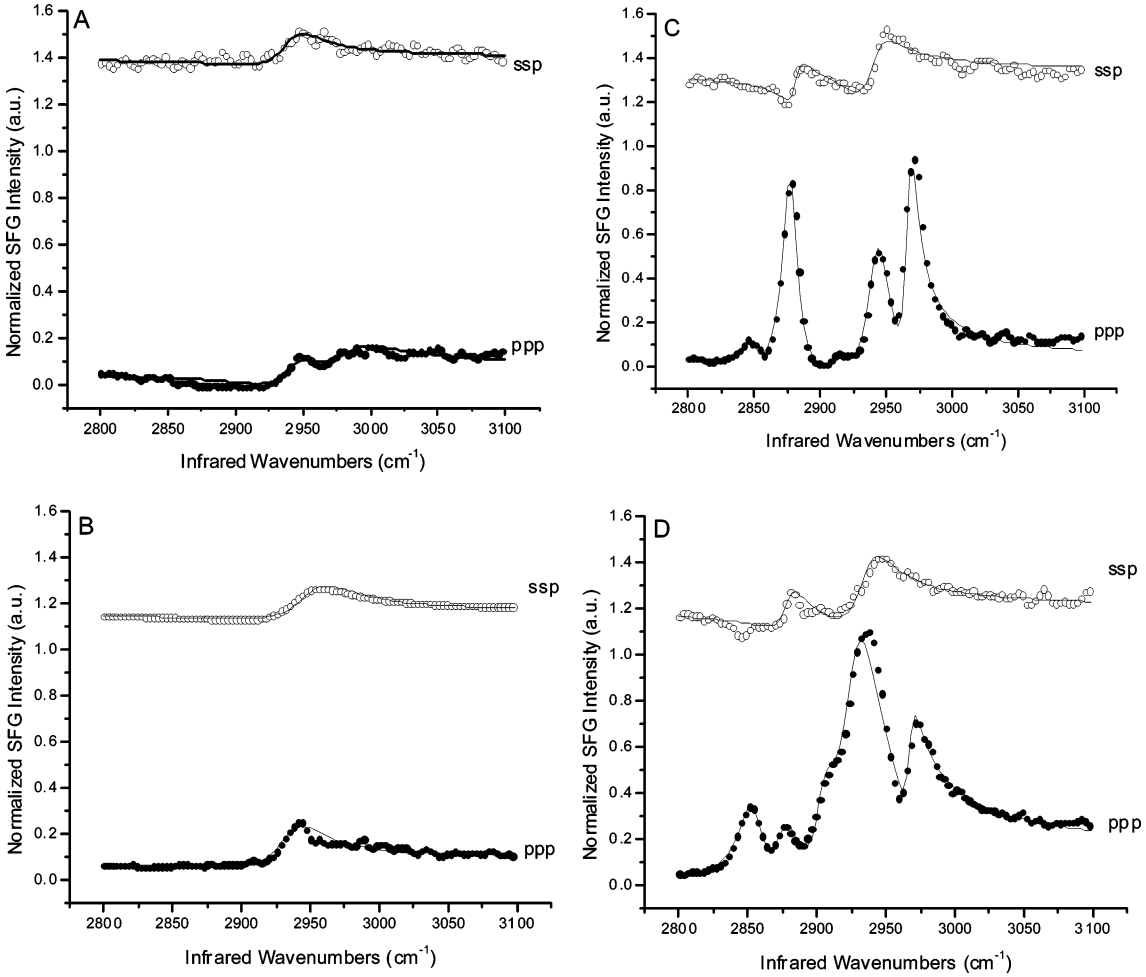

Figure 6. SFG spectra of freshly polished mild steel electrodes in air: (A) immersion in 0.1 M LiCl/CH_3OH solution with 1 mM ODT at OCP for 1−2 h; (B) immersion in 0.1 M LiCl/CH_3OH solution at −1.1 V for 1−2 h; (C) immersion in 0.1 M LiCl/CH_3OH solution with 1 mM ODT at −1.1 V for 1−2 h; (D) immersion in 0.1 M LiCl/CH_3OH solution with 1 mM ODT at −1.1 V for 1−2 h, then immersion in water purged with N_2 at OCP for 0.5 h. The solid line is the curve of fit on eq 1. The ssp spectra have been offset vertically by 1.1 for clarity.

our experimental condition. Moreover, these results also reveal that hydrocarbon contamination in the laboratory does not introduce a comparable SFG signal on the MS surface.

Figure 6C shows the typical SFG spectra of an ODT monolayer modified MS surface. It features three strong resonant peaks at 2877, 2943, and 2967 cm^{-1}, and two weak peaks at 2850 and 2914 cm^{-1}, respectively. The strong peaks at 2877, 2943, and 2967 cm^{-1} can be attributed to the terminal methyl groups of ODT molecules which point away from the surface. They are respectively assigned to symmetric, Fermi resonance, and antisymmetric CH stretching of the CH_3 group as in the case of ODT/Au. [41,44,77] The presence of the weak vibrational modes of the CH_2 groups in the SFG spectra suggests the presence of a defect in the monolayer.[39−41] It implies that the ODT monolayer at a MS surface is not packing as densely as it is at a Au surface. The phase angles of the nonresonant susceptibilities, based on the fitting parameters, are ∼45° for ppp and ∼15° for ssp SFG spectra, respectively.

In solutions without thiol, thiolates may desorb from the substrate due to a concentration difference between solution and substrate, leading to the formation of the defects and reorganization in monolayers.[17] However, highly ordered thiol monolayers at Au and Ag surfaces are quite stable in water since water is a poor solvent for most thiol compounds.[17,40,41] It is also observed that water does not perturb the SFG spectrum of alkanethiol monolayers on a Au surface (not shown). In the case of ODT/MS, it was found that water has significant impact on the SFG spectrum of the ODT monolayers at the MS surface. Shown in Figure 6D is the SFG spectra of an ODT/MS electrode that was recorded in air after immersion for 0.5 h in water purged with nitrogen gas flow. The intensities of the CH_3 modes at 2877 and 2973 cm^{-1} were dramatically reduced, whereas the relative intensities of the CH_2 modes at 2854 and 2910 cm^{-1} obviously increased compared to Figure 6C, indicating an increase in gauche defects in the ODT monolayer.

These results show that ODT monolayers on MS surfaces are not good barriers. The presence of defects in the ODT monolayer made it possible for water to penetrate into the film and reach the MS surface. Consequently, slow corrosion occurred at the MS surface since the water is slightly acidic (pH 5.8) even though the water was kept purged with N_2 gas during our experiment. Acidic water is corrosive to mild steel even if it is oxygen-free.[78] Corrosion may lead to ODT desorption from the MS surface, resulting in loose packing and increasing the tilt angle of the hydrocarbon chain. We have to note that the peak at 2936 cm^{-1} became unusually strong after being immersed in water for 0.5 h. Although the root cause for this change is not clear yet, it seems it is related to the corrosion effect. One possible reason might be the presence of decomposition products from the film, leading to a sharp increase of the resonance at 2936 cm^{-1}. It was found that the SFG spectrum of MS covered with an oxide layer showed a similar shape and intensity around 2936 cm^{-1} (not shown). On the other hand, CVs (see Figure 3) also show that the ODT monolayer did not

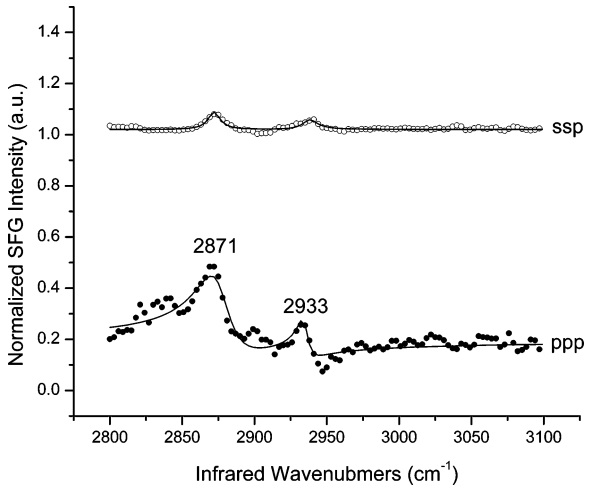

Figure 7. SFG spectra of an ODT monolayer modified mild steel electrode in water. The solid line is the curve of fit on eq 1. The spectra have been offset vertically for clarity.

TABLE 1: Refractive Index of Gold and Iron

refractive index	gold	iron
IR @ 2904 cm^{-1}	$2.046 + 21.3i$	$4.68 + 10.44i$
visible @ 539 nm	$0.402 + 2.54i$	$2.65 + 3.34i$
SFG @ 459.2 nm	$1.426 + 1.846i$	$2.23 + 3.25i$

completely block the charge transfer between the MS surface and solution. The ODT monolayer only delayed, not blocked, the oxidization of MS (onset oxidization potential shifted positively +150 mV), indicating the presence of defects in film.

Figure 7 is the SFG spectra of an ODT/MS in water. The SFG electrochemical cell was filled with deaerated water, and the electrode surface was pressed tightly to the IR quartz window where only a small amount of current was able to pass. In this case, the corrosion rate was quite slow, and it had no considerable influence on the MS surface during the experiment period. Therefore, only the interaction between the ODT chains and the water molecules that get into the film defects is considered. The ppp spectrum is dominated by symmetric and Fermi resonances of the CH_3 group. A similar effect of water on the orientation of ODT at the Pt surface has been observed by Hines et al.[40] As water gets into the ODT layer, the hydrophobic alkyl chains have to adopt a more close-packed configuration to reduce the repelling force from water. This means that ODT at mild steel has a smaller tilt angle in water than that in air. That is because only the symmetric and Fermi resonance of the methyl group can be observed with no antisymmetric resonance appearing in the ppp SFG spectrum. However, the resonance intensity in water is weaker than that in air, indicating there are more oriented but fewer ODT domains present at the MS surface in water. The shape of the ssp spectrum in water featured an obvious nonresonant phase shift compared to the spectra in air; one of the reasons might be the change of the electronic state of the mild steel induced by permeated water. The potential dependent SFG experiment currently being carried out will possibly reveal more detail about this problem.

3.6. SFG Orientation Calculation. A detailed description of the orientation calculation for the solid/air interface of ODT/Au and ODT/MS is described herein. Refractive indices used in calculating the Fresnel coefficients are listed in Table 1. Values for the refractive index of mild steel at the desired wavelengths are not available within the literature; therefore the numbers used were for iron. The value used for n_m at all wavelengths was the macroscopic refractive index of ODT, 1.4648.[79] The optical Fresnel coefficients calculated for the gold/air and iron/air systems are listed in Tables 2 and 3, respectively.[80,81] Calculation of the hyperpolarizability tensors for the methyl stretching modes were done by the method outlined by Hirose et al.[36,82,83] using a value of 0.6 as the dipole derivative[84] and 1.44 as the polarizabilty derivative.[85]

TABLE 2: Fresnel Coefficients for Gold/Air Interface with $n' = 1.4648$

	K_{xx}	K_{yy}	K_{zz}
IR	$-0.017 + 0.090i$	$0.0055 - 0.046i$	$-0.79 - 0.073i$
visible	$-0.39 + 0.52i$	$0.19 - 0.457i$	$-0.4766 + 0.244i$
SFG	$0.501 - 0.298i$	$0.35 - 0.334i$	$-0.43 - 0.148i$

TABLE 3: Fresnel Coefficients for Iron/Air Interface $W/n' = 1.4648$

	K_{xx}	K_{yy}	K_{zz}
IR	$-0.087 + 0.136i$	$0.0379 - 0.077i$	$-0.737 - 0.110i$
visible	$-0.296 + 0.238i$	$0.208 - 0.213i$	$-0.521 - 0.111i$
SFG	$0.309 - 0.265i$	$0.205 - 0.235i$	$-0.526 - 0.13i$

TABLE 4: Ratio of Intensity of SFG Signal with Instrumental Efficiency Accounted for

	gold	mild steel
sym SSP/sym PPP	0.255 ± 0.03	
sym SSP/asym PPP	6.41 ± 1.6	
sym PPP/asym PPP	21.4 ± 4.86	4.4 ± 1.1

To correctly calculate the intensity ratios which are used to determine the angle of orientation, the amount of intensity shared by the fundamental methyl symmetric vibration and the Fermi resonance must be taken into account. Since the Fermi resonance is an overtone vibration, thus its probability is very low, all of the intensity of the Fermi resonance vibration is considered to be "stolen" from the fundamental and included into its intensity for the orientation calculations. Differences in reflection efficiency for s- and p-polarized light caused an instrumental correction which had to be taken into account. The ratio of instrumental loss for the two polarization combinations ssp/ppp was equal to 2.7. To correctly compare the intensities of the resonances, the amplitudes determined from the curve fitting were divided by the peak widths and squared.[86,87] Where I, A,

$$I = \left(\frac{A}{\Gamma}\right)^2 \tag{29}$$

and Γ are equal to the intensity, amplitude, and peak width, respectively. After taking into account the effects of the Fermi resonance, instrumental corrections, and normalization of peak widths, the intensity ratios of the resonances are list in Table 4. When these values are plotted against the curves shown in Figures 9−12 the tilt angle of the methyl group was determined. Each plot contains three curves; the solid lines are for an n' value of the bulk refractive index of ODT. Due to the ambiguity of n', the dotted and dashed lines are for values above and below the bulk refractive index. Because the resonances of the methyl group are not convoluted with other peaks for the ODT/Au system all three curves plotted in Figures 9−11 have the ability to correctly calculate the orientation of the methyl group at the surface. When all three orientation curves for the ODT/Au system are examined, the overlap yields a tilt angle of the methyl group of 30 ± 3° from normal. This is consistent with the previous results that the molecular chain tilt angle, chain twist angle, and methyl group tilt angle for the $CH_3(CH_2)_nSH$ (here n is odd) molecules adsorbed on the Au(111) surface are 30°, 50°, and 27°, respectively.[88] By the use of the same calculation, only changing the optical constants for iron instead of gold, orientation curves for the ODT/MS surface were generated.

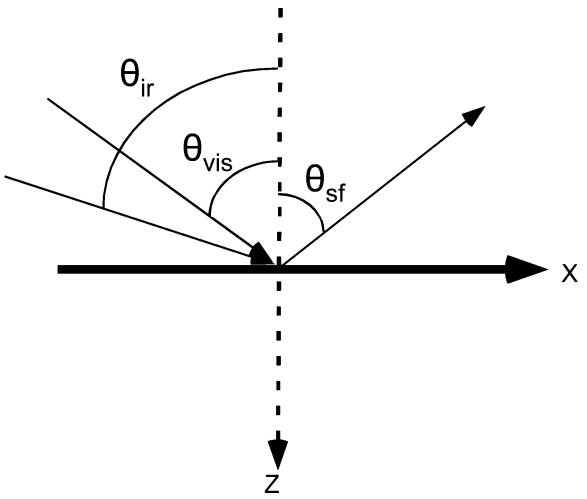

Figure 8. Coordinate system of SFG setup.

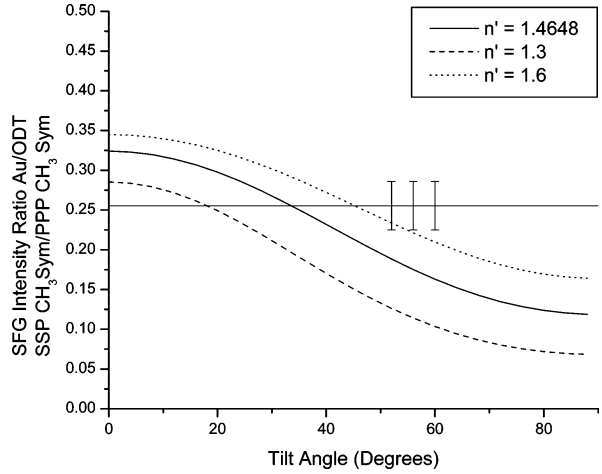

Figure 9. Simulation of SFG signal as a function of methyl group orientation on gold/ODT interface.

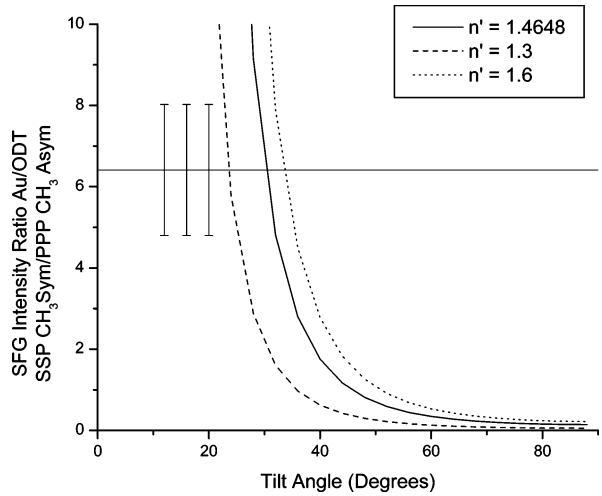

Figure 10. Simulation of SFG signal as a function of methyl group orientation on gold/ODT interface.

When the ssp spectra of the ODT/MS system were curve fit, the amplitude for the resonance attributed to the Fermi resonance was larger than the amplitude of the fundamental symmetric stretch. This led us to believe that there was some other contribution to this peak, because a Fermi resonance cannot have more intensity than the fundamental stretch.[89] The ppp spectra signal level is much higher than that of the ssp spectra and does not seem to be influenced. Therefore only the ppp spectrum was used for the orientation calculation of the ODT/MS system.

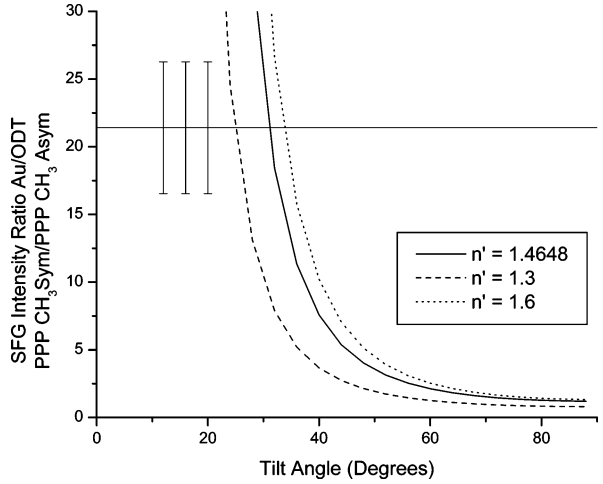

Figure 11. Simulation of SFG signal as a function of methyl group orientation on gold/ODT interface.

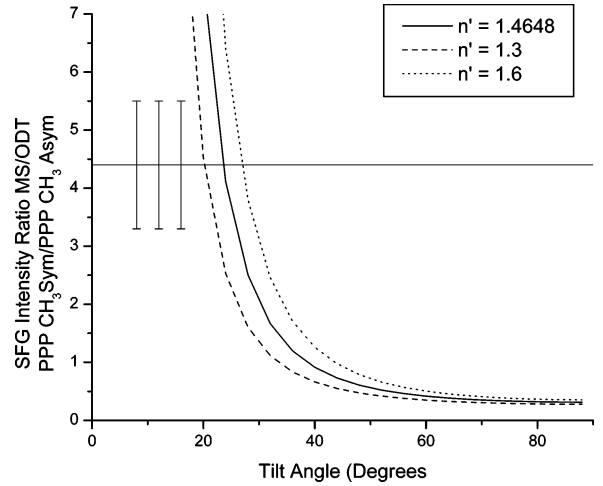

Figure 12. Simulation of SFG signal as a function of methyl group orientation on mild steel/ODT interface.

The orientation curve for the ODT/MS surface is plotted in Figure 12. The curve yields a tilt angle of the methyl group of $23 \pm 3°$ from the surface normal. Because the refractive index values can greatly affect the orientation predicted by these calculations, the optical constants for iron may not describe the MS surface correctly; therefore the orientation of ODT on MS is only an estimated value.

SFG and impedance provide two distinct methods to determine the orientation on the monolayer film of ODT. The impedance provides the average molecular chain tilt angle based on the thickness of a barrier layer at the interface, while SFG gives the terminal methyl group's tilt angle which is the angle between the terminal C−C bond axis and the surface normal. The simple mechanical orientation calculation from impedance data took the geometric area of the Au and MS electrodes as the real surface areas without considering the impact of the roughness on the surface area. Actually, in these experiments, the Au electrode was polished to 0.05 μm with Al_2O_3 paste, while the MS electrode was only polished to 1 μm with diamond paste. Therefore, the real surface area of MS (A_{MS}) was greater than that of the Au (A_{Au}) electrode resulting in the calculated $\theta_{ODT/MS}$, based on eq 28, which was greater than the real $\theta_{ODT/MS}$. Although it is not easy to evaluate the roughness factor of the MS electrode, it can be estimated in our case that a 6°

difference for calculated $\theta_{ODT/MS}$ will be introduced by 0.1 difference of roughness factor between the Au and MS electrodes.

On the other hand, the appearance of resonances from methylene groups in SFG spectrum shows that there is evidence of gauche defects in the monolayer on MS. The presence of gauche defects will reduce the chain length (l) of the adsorbed ODT molecules as shown in Figure 4. From eqs 23 and 26, in the case of C_m being fixed (which also means d is fixed), we have

$$\cos \alpha = \frac{d}{l} = \frac{\epsilon\epsilon_0}{lC_m} \propto \frac{1}{l} \tag{30}$$

It is obvious that reduction in the effective chain length will lead to a reduction in tilt angle (α). To illustrate how the gauche defects impact the calculation of α, we consider the simplest model: There is only one gauche defect present in the adsorbed ODT chain. The contribution of per CH_3 or CH_2 group to the chain length along molecular axis is about 0.13 nm due to the 0.154 nm C−C bond length and the 109.5° C−C−C angle. The effect of the presence of one gauche defect can be roughly taken as canceling one C−C bond's contribution to the chain length. The reduction in chain tilt angle (α) per gauche defect can then be estimated as 4° in the case of ODT monolayer on the MS surface.

There are three parameters used in the description of long alkyl chains on surfaces, the methyl group's tilt angle (θ), the chain tilt angle (α), and the chain twist angle (β).The methyl group's tilt angle (θ) can be determined from SFG. The chain tilt angle has been determined from capacitance measurements using impedance spectroscopy. Assuming the alkyl chain is in an all-trans extended conformation and then, From a purely geometric viewpoint, determination of the twist angle (β) is possible. Hence, SFG combining impedance provides an approach to determine the orientation parameters of the adsorbates on the metal electrode surface. For the ODT/MS system this was not possible because of the gauche defects in the monolayer which make an accurate description of the monolayer unfeasible.

Conclusions

ODT monolayers were self-assembled at MS electrode surfaces in a 0.1 M $LiCl/CH_3OH$ solution under cathodic polarization.

1. CV and SFG spectra revealed that the adsorption of the ODT at an oxide layer covered MS surface is so weak that it could not form well-defined monolayers. Under cathodic polarization (−1.2 to −1.1 V vs SCE), ODT strongly adsorbed at an oxide-free MS surface and formed a densely packed and oriented monolayer, featured by a dramatic drop in charging current in the CV curve, a peak of S_{2p} binding energy at 162.1 eV in XPS spectrum, and the appearance of three strong CH_3 group peaks (2877, 2943, and 2967 cm^{-1}) in the SFG spectra. However, the presence of the two weak peaks at 2950 and 2914 cm^{-1} in the ppp SFG spectrum indicates there are some defects in ODT monolayer at the MS surface. It implies that ODT molecules do not pack as densely as they do on a gold surface. It is therefore possible for solution to penetrate through the defects to reach the MS surface. Water was found to significantly impact the ODT monolayers on mild steel. In water, the SFG spectra of ODT/MS electrode were characterized by a red shift in frequencies and nonresonant phase change.

2. On the basis of the EIS data of a MS electrode, the fit parameter, C_m, for the ODT monolayer was equal to 2.52 $\mu F/cm^2$, that is consistent with the typical value of the thiol monolayer formed at noble metal. Through the use of a simple geometric model, the chain tilt angle of the ODT molecules at mild steel was deduced from the fit capacitance value as ∼48°. This value is greater than the typical value for ODT/Au (30°).

3. Orientation calculations for the SFG result from the air/solid interface of both the ODT/Au and ODT/MS interfaces. The orientation calculated for the ODT/Au interface corresponded well with previous studies within the literature. Calculation of the ODT/MS interface yielded an orientation of 23 ± 3° from the surface normal.

Acknowledgment. This work is based in part upon work supported by Texas Advanced Technology Program (ATP) under Grant Number 003652-0044-2003. We are also grateful to Champion Technologies (Houston) for support and encouragement in this project.

References and Notes

(1) Laibinis, P. E.; Whitesides, G. M.; Allara, D. L.; Tao, Y. T.; Parikh, A. N.; Nuzzo, R. G. *J. Am. Chem. Soc.* **1991**, *113*, 7152.
(2) Kim, Y. T.; McCarley, R. L.; Bard, A. J. *J. Phys. Chem.* **1992**, *96*, 7416.
(3) Fenter, P.; Eberhardt, A.; Eisenberger, P. *Science* **1994**, *266*, 1216.
(4) McDermott, C. A.; McDemott, M. T.; Green, J. B.; D., P. M. *J. Phys. Chem.* **1995**, *99*, 13257.
(5) Sigal, G. B.; Bamdad, C.; Barberis, A.; Strominger, J.; Whitesides, G. M. *Anal. Chem.* **1996**, *68*, 490.
(6) Poirier, G. E. *Langmuir* **1997**, *13*, 2019.
(7) Ron, H.; Cohen, H.; Matlis, S.; Rappaport, M.; Rubinstein, I. *J. Phys. Chem. B* **1998**, *102*, 9861.
(8) Byloos, M.; Al-Maznai, H.; Morin, M. *J. Phys. Chem. B* **1999**, *103*, 6554.
(9) Zhang, H. P.; Luo, J.; Huang, H. G.; Wu, L. L.; Lin, Z. H. *Chem. Phys. Lett.* **2000**, *326*, 169.
(10) Duan, L.; Garrett, S. J. *J. Phys. Chem. B* **2001**, *105*, 9812.
(11) Liu, D.; Szulczewski, G. J.; Kispert, L. D.; Primak, A.; Moore, T. A.; Moore, A. L.; Gust, D. *J. Phys. Chem. B* **2002**, *106*, 2933.
(12) Yang, X.; Perry, S. S. *Langmuir* **2003**, *19*, 6135.
(13) Ulman, A. *Chem. Rev.* **1996**, *96*, 1533.
(14) Lavrich, D. J.; Wetterer, S. M.; Bernasek, S. L.; Scoles, G. *J. Phys. Chem. B* **1998**, *102*, 3456.
(15) Laibinis, P. E.; Whitesides, G. M. *J. Am. Chem. Soc.* **1992**, *114*, 1990.
(16) Childs, W. R.; Nuzzo, R. G. *Langmuir* **2005**, *21*, 195.
(17) Schlenoff, J. B.; Li, M.; Ly, H. *J. Am. Chem. Soc.* **1995**, *117*, 12528.
(18) Walczak, M. M.; Chung, C.; Stole, S. M.; Widrig, C. A.; Porter, M. D. *J. Am. Chem. Soc.* **1991**, *113*, 2370.
(19) Osawa, M.; Matsuda, N.; Yoshii, K.; Uchida, I. *J. Phys. Chem.* **1994**, *98*, 12702.
(20) Lang, P.; Mekhalif, Z.; Rat, B.; Garnier, F. *J. Electroanal. Chem.* **1998**, *441*, 83.
(21) Brito, R.; Tremont, R.; Cabrera, C. R. *J. Electroanal. Chem.* **2004**, *574*, 15.
(22) Li, Z.; Chang, S.-C.; Williams, R. S. *Langmuir* **2003**, *19*, 6744.
(23) Laibinis, P. E.; Whitesides, G. M. *J. Am. Chem. Soc.* **1992**, *114*, 9022.
(24) Jennings, G. K.; Yong, T. H.; Munro, J. C.; Laibinis, P. E. *J. Am. Chem. Soc.* **2003**, *125*, 2950.
(25) Volmer, M.; Stratmann, M.; Viefhaus, H. *Surf. Interface Anal.* **1990**, *16*, 278.
(26) Volmer-Uebing, M.; Stratmann, M. *Appl. Surf. Sci.* **1992**, *55*, 19.
(27) Kataby, G.; Prozorov, T.; Koltypin, Y.; Cohen, H.; Sukenik, C. N.; Ulman, A.; Gedanken, A. *Langmuir* **1997**, *13*, 6151.
(28) Grundmeier, G.; Reinartz, C.; Rohwerder, M.; Stratmann, M. *Electrochim. Acta* **1998**, *43*, 165.
(29) Nozawa, N.; Aramaki, K. *Corros. Sci.* **1999**, *41*, 57.
(30) Ruan, C. M.; Bayer, T.; Meth, S.; Sukenik, C. N. *Thin Solid Films* **2002**, *419*, 95.
(31) Whelan, C. M.; Barnes, C. J.; Walker, C. G. H.; Brown, N. M. D. *Surf. Sci.* **1999**, *425*, 195.
(32) Whelan, C. M.; Smyth, M. R.; Barnes, C. J. *Langmuir* **1999**, *15*, 116.
(33) Barner, B. J.; Corn, R. M. *Langmuir* **1990**, *6*, 1023.
(34) Anderson, M. R.; Gatin, M. *Langmuir* **1994**, *10*, 1638.

(35) Shon, Y. S.; Colorado, R.; Williams, C. T.; Bain, C. D.; Lee, T. R. *Langmuir* **2000**, *16*, 541.
(36) Hirose, C.; Akamatsu, N.; Domen, K. *J. Chem. Phys.* **1992**, *96*, 997.
(37) Hirose, C.; Yamamoto, H.; Akamatsu, N.; Domen, K. *J. Phys. Chem.* **1993**, *97*, 10064.
(38) Ward, R. N.; Davies, P. B.; Bain, C. D. *J. Phys. Chem.* **1993**, *97*, 7141.
(39) Ward, R. N.; Duffy, D. C.; Davies, P. B.; Bain, C. D. *J. Phys. Chem.* **1994**, *98*, 8536.
(40) Hines, M. A.; Todd, J. A.; Guyot-Sionnest, P. *Langmuir* **1995**, *11*, 493.
(41) Bain, C. D. *J. Chem. Soc., Faraday Trans.* **1995**, *91*, 1281.
(42) Bell, G. R.; Bain, C. D.; Ward, R. N. *J. Chem. Soc., Faraday Trans.* **1996**, *92*, 515.
(43) Duffy, D. C.; Friedmann, A.; Boggis, S. A.; Klenerman, D. *Langmuir* **1998**, *14*, 6518.
(44) Tanaka, Y.; Lin, S.; Aono, M.; Suzuki, T. *Appl. Phys. B* **1999**, *68*, 713.
(45) Zhuang, X.; Miranda, P. B.; Kim, D.; Shen, Y. R. *Phys. Rev. B* **1999**, *59*, 12632.
(46) Baldelli, S.; Markovic, N.; Ross, P. N.; Shen, Y. R.; Somorjai, G. A. *J. Phys. Chem. B* **1999**, *103*, 8920.
(47) Himmelhaus, M.; Disert, F.; Buck, M.; Grunze, M. *J. Phys. Chem.* **2000**, *104*, 576.
(48) Buck, M.; Himmelhaus, M. *J. Vac. Sci. Technol., A* **2001**, *19*, 2717.
(49) Baldelli, S.; Mailhot, G.; Ross, P. N.; Somorjai, G. A. *J. Am. Chem. Soc.* **2001**, *123*, 7697.
(50) Watry, M. R.; Richmond, G. L. *J. Phys. Chem. B* **2002**, *106*, 12517.
(51) Chou, K. C.; Kim, J.; Baldelli, S.; Somorjai, G. A. *J. Electroanal. Chem.* **2003**, *554*−*555*, 253.
(52) Baldelli, S. *J. Phys. Chem. B* **2003**, *107*, 6148.
(53) Rivera-Rubero, S.; Baldelli, S. *J. Phys. Chem. B* **2004**, *108*, 15133.
(54) Rivera-Rubero, S.; Baldelli, S. *J. Am. Chem. Soc.* **2004**, *126*, 11788.
(55) Maechling, C. R.; Kliner, D. A. V.; Klenerman, D. *Appl. Spectrosc.* **1993**, *47*, 167.
(56) Westerberg, S.; Wang, C.; Chou, K.; Somorjai, G. A. *J. Phys. Chem. B* **2004**, *108*, 6374.
(57) Feller, M. B.; Chen, W.; Shen, Y. R. *Phys. Rev A* **1991**, *43*, 6778.
(58) Miranda, P. B.; Shen, Y. R. *J. Phys. Chem. B* **1999**, *103*, 3292.
(59) Wei, X.; Hong, S.; Zhuang, X.; Shen, Y. R. **2000**.
(60) Bell, G. R.; Li, Z. X.; Bain, C. D. *J. Phys. Chem. B* **1998**, *102*, 9461.
(61) Braun, R.; Casson, B. D.; Bain, C. D. *J. Chem. Phys.* **1999**, *110*, 4634.
(62) Hirose, C.; Akamatsu, N.; Domen, K. *Appl. Spectrosc.* **1992**, *46*, 1051.
(63) Janek, R. P.; Fawcett, W. R.; Ulman, A. *J. Phys. Chem. B* **1997**, *101*, 8550.
(64) Protsailo, L. V.; Fawcett, W. R. *Electrochim. Acta* **2000**, *45*, 3497.
(65) Subramanian, R.; Lakshminarayanan, V. *Electrochim. Acta* **2000**, *45*, 4501.
(66) Schweiss, R.; Werner, C.; Knoll, W. *J. Electroanal. Chem.* **2003**, *540*, 145.
(67) Finklea, H. O. In *Electroanalytical Chemistry, A series of Advances*; Bard, A. J., Rubinstein, I., Eds.; Marcel Dekker: New York, 1996; Vol. 19; pp 166−167.
(68) Hsu, C. H.; Mansfeld, F. *Corrosion* **2001**, *57*, 747.
(69) Harris, A. L.; Chidseg, C. E. D.; Levinos, N. J.; N., L. D. *Chem. Phys. Lett.* **1987**, *141*, 350.
(70) Bain, C. D.; Davies, P. B.; Ong, T. H.; Ward, R. N.; Brown, M. A. *Langmuir* **1991**, *7*, 1563.
(71) Campion, A. *Annu. Rev. Phys. Chem.* **1985**, *36*, 549.
(72) Sellers, H.; Ulman, A.; Shnidman, Y.; Eilers, J. E. *J. Am. Chem. Soc.* **1993**, *115*, 9389.
(73) Feng, Y. Q.; Teo, W. K.; Siow, K. S.; Gao, Z. Q.; Tan, K. L.; K., H. A. *J. Electrochem. Soc.* **1997**, *144*, 55.
(74) Ma, H. Y.; Yang, C.; Chen, S. H.; Jiao, Y. L.; Huang, S. X.; Li, D. G.; Luo, J. L. *Electrochim. Acta* **2003**, *48*, 4277.
(75) Dubois, L. H.; Nuzzo, R. G. *Annu. Rev. Phys. Chem.* **1992**, *43*, 437.
(76) Love, J. C.; Estroff, L. A.; Kriebel, J. K.; Nuzzo, R. G.; Whitesides, G. M. *Chem. Rev.* **2005**, *105*, 1103.
(77) Dreesen, L.; Humbert, C.; Celebi, M.; Lemaire, J. J.; Mani, A. A.; Thiry, P. A.; Peremans, A. *Appl. Phys. B* **2002**, *74*, 621.
(78) Davis, J. R. *Surface Engineering for Corrosion and Wear Resistance*; ASM International: Materials Park, OH, 2001.
(79) Dean, J. A. *Lange's Handbook of Chemistry*; McGraw-Hill: New York, 1992.
(80) Weast, R. C. *CRC Handbook of Chemistry and Physics*; CRC Press: Boca Raton, FL, 1984.
(81) *Handbook of Optical Constants of Solids*; Palik, E. D., Ed.; Academic Press: San Diego, CA, 1998.
(82) Bunker, P. R. *Molecular symmetry and spectroscopy*; Academic: New York, 1970.
(83) Wilson, E. B.; Decius, J. C.; Cross, P. C. *Molecular vibrations*; McGraw-Hill: New York, 1955.
(84) Snyder, R. G. *J. Chem. Phys.* **1965**, *42*, 1744.
(85) Gough, K. M.; Murphy, W. F. *J. Chem. Phys.* **1987**, *87*, 3341.
(86) McHale, J. L. *Molecular Spectroscopy*; Prentice Hall: Englewood Cliffs, New Jersey, 1999.
(87) Demtroder, W. *Laser Spectroscopy*; Springer: New York, 1996.
(88) Nishi, N.; Hobara, D.; Yamamoto, M.; Kakiuchi, T. *J. Chem. Phys.* **2003**, *118*, 1904.
(89) Herzberg, G. *Molecular spectra and molecular structure*; D. Van Nostrand Company: New York, 1945.